Equation of state of the α-PbO_2 and $Pa\bar{3}$-type phases of GeO_2 to 120 GPa

R. Dutta,[1,*] C. E. White,[2,3] E. Greenberg,[4] V. B. Prakapenka,[4] and T. S. Duffy[1]
[1]*Department of Geosciences, Princeton University, Princeton, New Jersey 08544, USA*
[2]*Department of Civil and Environmental Engineering, Princeton University, Princeton, New Jersey 08544, USA*
[3]*Andlinger Center for Energy and the Environment, Princeton University, Princeton, New Jersey 08544, USA*
[4]*Center for Advanced Radiation Sources, University of Chicago, Chicago, Illinois 60637, USA*

(Received 14 June 2018; revised manuscript received 27 August 2018; published 11 October 2018)

The compression behavior of crystalline and amorphous germania holds considerable interest as an analog for silica and for understanding the structural response of AX_2 compounds generally. In this paper, the α-PbO_2-type and $Pa\bar{3}$-type polymorphs of GeO_2 were investigated under high pressure using angle-dispersive synchrotron x-ray diffraction in the laser-heated diamond anvil cell. Theoretical calculations based on density functional theory were also performed. The experimental pressure-volume data were fitted to third-order Birch-Murnaghan equations of state. The fit parameters for the α-PbO_2 type are $V_0 = 53.8\,(2)$ Å^3, $K_{0T} = 293\,(7)$ GPa with fixed $K'_{0T} = 4$, where V, K_T, and K'_T are the volume, isothermal bulk modulus, and pressure derivative of the bulk modulus and the subscript zero refers to ambient conditions. The corresponding parameters for the $Pa\bar{3}$-type phase are $V_0 = 50.3\,(3)$ Å^3, $K_{0T} = 342\,(12)$ GPa with fixed $K'_{0T} = 4$. The theoretical calculations are in good agreement with the experimental results with slight underestimation and overestimation of V_0 and K_{0T}, respectively. A theoretical Hugoniot was calculated from our data and compared to shock equation of state data for vitreous and rutile-type GeO_2. The high-pressure phase observed on the Hugoniot is most consistent with either the α-PbO_2-type or $CaCl_2$-type phase. Finally, we have compared our data on crystalline germania with existing studies on the corresponding phases of SiO_2 to better understand the effects of cation substitution on phase transformations and equations of state in group 14 dioxides.

DOI: 10.1103/PhysRevB.98.144106

I. INTRODUCTION

The crystalline and vitreous forms of germania, GeO_2, have been extensively studied using a wide range of static and dynamic compression techniques [1–3]. The structure of amorphous germania at high pressure has been examined using x-ray-absorption spectroscopy [4–7], Raman [8] and infrared spectroscopy [9], as well as x-ray [10–13] and neutron diffraction [14–16]. Static compression experiments on crystalline GeO_2 have concentrated on the high-pressure crystal structure [17–19] and phase transitions [20–22]. Dynamic compression experiments [1,2,23–25] have also been carried out on germania crystals and glass. There have also been a number of theoretical studies [26–29] investigating the high-pressure behavior of the different phases of this material.

The long-standing interest in GeO_2 is due in part to its role as a structural analog for SiO_2. Silica is the most abundant oxide component of the earth's crust and mantle. High-pressure experiments and theoretical calculations show that the phase transition sequence in SiO_2, starting from rutile type (stishovite), is $CaCl_2$ type [30,31] (60 GPa) to α-PbO_2 type (seifertite) [32] (121 GPa) to $Pa\bar{3}$ type [33] (sometimes referred to as pyrite type) (268 GPa). Density functional calculations have predicted a further transition from the $Pa\bar{3}$-type structure to a Fe_2P-type [34] structure at 640 GPa or cotunnite [35] (α-$PbCl_2$)-type structure around 700 GPa. Although the ultra-high-pressure phases are not expected to be stable in the Earth's interior, they may be key components of large, rocky extra-solar planets [36]. A large number of additional studies [37–41] have also focused on the high-pressure behavior of silica glass to understand the structural and coordination number changes it undergoes as a function of static and dynamic compression.

The extreme pressures required for phase transitions in SiO_2 make it very challenging to study many of these phases experimentally, necessitating the use of analogs [3,42–44]. At pressures above 1 Mbar (100 GPa), it is difficult to maintain thermally uniform conditions in laser-heated diamond anvil cells. GeO_2 follows a similar sequence of phase transitions as SiO_2, but the phase transitions occur at lower pressures due to the larger ionic radius of Ge^{4+} compared with Si^{4+}. This facilitates the use of thicker samples and insulating layers in the diamond anvil cell and more controlled heating conditions.

Under room-temperature compression, α-quartz-type germania has been reported to undergo pressure-induced amorphization [45] or form a disordered monoclinic ($P2_1/c$) phase above 6 GPa [18]. Rutile-structured germania ($P42/mnm$) undergoes a phase transition to the orthorhombic $CaCl_2$ type ($Pnnm$) near 26 GPa with a positive Clapeyron slope [20]. This is followed by transitions to the α-PbO_2-type ($Pbcn$) phase near 36 GPa [21] and the $Pa\bar{3}$-type phase near 65 GPa [26] (theory) or 90 GPa [46]. No further phase transitions are observed up to 130 GPa [19]. First-principles calculations [29] predict the $Pa\bar{3}$-type to cotunnite-type and cotunnite-type to

*rd7@princeton.edu

 ©2018 American Physical Society

Fe_2P-type phase transitions to occur at ∼300 and ∼600 GPa, respectively.

For glasses and liquids, GeO_2 is used to model the response of tetrahedral-network glasses and their evolution from corner-sharing tetrahedra at ambient pressure to a dense octahedrally coordinated glass at high pressures [7,10,47]. It has been suggested based on molecular dynamics simulations that GeO_2 glass undergoes multiple amorphous-amorphous transitions that have direct parallels to their crystalline counterparts under pressure [48]. Recent extended x-ray-absorption fine-structure and x-ray-absorption near-edge structure spectra on dense GeO_2 glass show evidence for changes in bond distance and coordination number increase at high pressure above 45 GPa [7]. Shock-wave compression of vitreous and crystalline rutile-type GeO_2 suggest a common high-pressure phase (HPP) or a phase with ∼5% higher zero-pressure density (with respect to rutile) above 35 and 70 GPa, respectively [1].

Much of the existing work on high-pressure GeO_2 crystalline phases is fragmentary, and there are limited experimental data above 50 GPa. In this paper, we have performed laser-heated diamond anvil cell experiments and *ab initio* calculations to obtain the 300-K (0 K for theoretical calculations) equation of state (EOS) of the α-PbO_2- and $Pa\bar{3}$-type phases of GeO_2 to 120 GPa. We have compared our pressure-volume data with previous studies for both SiO_2 and GeO_2. We have also compared our results with shock compression data to better identify possible candidates for the high-pressure Hugoniot phase(s).

A. Experimental procedure

Polycrystalline GeO_2 (Aldrich, >99.998% purity) was examined at ambient conditions using synchrotron x-ray diffraction and was found to be in the α-quartz structure with lattice parameters $a = 4.963\,(1)$ Å, $c = 5.638\,(3)$ Å, in good agreement with literature values [49]. The sample was ground to micron-sized grains under ethanol and mixed with 10-wt.-% platinum to serve as both the pressure calibrant and laser absorber. The sample + Pt mixture was then pressed into ∼7–10-μm-thick foils. Rhenium gaskets were preindented to ∼20–30-μm thickness and 60–120-μm-diameter holes were drilled to form the sample chamber. The sample foils were then loaded into symmetric diamond anvil cells with 100–200-μm culet diamond anvils mounted on tungsten carbide or cubic boron nitride seats. Three ruby balls (∼5-μm diameter) arranged in a triangular pattern were used to support the sample. Neon was loaded into the sample chamber using the gas-loading system at GeoSoilEnviroCARS, Sector 13 of the Advanced Photon Source (APS). Pressure was determined using the (111) diffraction peak and the EOS of Pt [50,51].

In situ angle-dispersive x-ray diffraction was carried out at beamline 13-ID-D of the APS using a monochromatic x-ray beam ($\lambda = 0.3344$ Å). The x rays were focused to a ∼3×3-μm spot size using Kirkpatrick-Baez mirrors. Diffraction patterns were collected using a two-dimensional 165 MAR-CCD or a CdTe 1M Pilatus detector. Lanthanum hexaboride (LaB_6) was used as a standard to calibrate the detector position and orientation.

X-ray-diffraction patterns were collected at 1–5-GPa intervals for 5–30 s. High-pressure phases were synthesized by heating from both sides using diode pumped fiber lasers [52] with a ∼15-μm spot size. The sample was annealed at ∼1200 K after each ∼5-GPa pressure step to relax differential stress. Temperatures were measured using spectroradiometry [53]. The laser power on each side was adjusted independently so that temperature differences between the upstream and downstream sides were less than 50 K. The two-dimensional images were integrated to obtain the one-dimensional x-ray patterns using the software DIOPTAS [54]. Peak positions were determined by fitting background-subtracted Voigt shapes to the data. Lattice parameters were calculated using least-squares refinement of the peak positions using the program UNITCELL [55].

B. Computational details

Total-energy calculations were performed using the plane-wave implementation of density functional theory [56,57] as implemented in the CASTEP [58] code. The exchange and correlation energies were treated using the local-density approximation (LDA). For all calculations, we used a kinetic-energy cutoff of 400 eV for the basis set. The Brillouin zone was sampled using a Monkhorst-Pack [59] 4×3×3 and 4 × 4 × 4k-point grid for the α-PbO_2- and $Pa\bar{3}$-type phases, respectively. Ultrasoft [60] pseudopotentials were used to treat the electron-ion interactions. The geometry optimizations were carried out using the Broyden-Fletcher-Goldfarb-Shanno [61] algorithm and were considered complete when the forces on atoms were less than 0.01 eV/Å and the energy change was less than 5×10^{-6} eV/atom. Both atomic positions and lattice parameters were optimized at each pressure step.

C. Data analysis

The pressure-volume data for the different phases were fit to an isothermal third-order Birch-Murnaghan (BM-3) EOS:

$$P(V) = \frac{3}{2}K_{0T}\left[\left(\frac{V_0}{V}\right)^{\frac{7}{3}} - \left(\frac{V_0}{V}\right)^{\frac{5}{3}}\right] \times \left\{1 + \frac{3}{4}(K'_{0T} - 4)\left[\left(\frac{V_0}{V}\right)^{\frac{2}{3}} - 1\right]\right\}, \quad (1)$$

where P is the pressure, K_T is the isothermal bulk modulus, K'_T is the pressure derivative of the bulk modulus, V is the unit-cell volume, and the subscript zero refers to ambient pressure. For the experimental data, K'_{0T} was fixed at 4 in performing the fit.

The presence of nonhydrostatic stresses can affect equation of state determination in a diamond anvil cell. To assess this, the differential stresses in the Pt pressure standard were evaluated using lattice strain theory [62]. Differential stress (t) results in variation in the lattice dimension as a function of crystallographic orientation (hkl) for elastically anisotropic crystals. For a crystal with cubic symmetry, the elastic anisotropy can be expressed using the anisotropy

factor, S:

$$S = \left(\frac{S_{11} - S_{12} - S_{44}}{2}\right), \tag{2}$$

where Sij are the single-crystal elastic compliances. The effect of deviatoric stress on the measured unit-cell parameter, a_m, for a given hkl can be expressed as [62,63]

$$a_m(hkl) = M_0 + M_1[3(1 - 3\sin^2\theta)\Gamma(hkl)], \tag{3}$$

where

$$M_0 = a_P\left\{1 + \frac{\alpha t}{3}(1 - 3\sin^2\theta)\left[S_{11} - S_{12} - \frac{1 - \alpha^{-1}}{2G_V}\right]\right\}, \tag{4}$$

$$M_1 = -\frac{a_P \alpha S t}{3}, \tag{5}$$

$$\Gamma(hkl) = \frac{h^2k^2 + k^2l^2 + l^2h^2}{(h^2 + k^2 + l^2)^2}. \tag{6}$$

a_P is the lattice parameter under hydrostatic pressure (P) only, α is a measure of continuity of stress and strain across grain boundaries, and θ is the scattering angle; α typically takes values between 0.5 and 1 but it has been suggested that it can exceed 1 in certain cases [64]. G_v is the Voigt limit of the shear modulus under isostrain conditions. Assuming $M_0 \approx a_P$ and $\alpha = 1$ [49,53], the product St can be derived directly from the slope and intercept of the Γ plot [$a_m(hkl)$ versus $3(1 - 3\sin^2\theta)\Gamma(hkl)$]:

$$St \approx \frac{3M_1}{M_0}. \tag{7}$$

The anisotropy factor of platinum as a function of pressure was obtained from theoretical calculations of Menéndez-Proupin and Singh [66].

We have also calculated a theoretical Hugoniot for GeO_2 using our experimental 300-K isotherm and the Mie-Grüneisen equation [67]. For any volume of interest, V, we compute the pressure along the principal isentrope, $P_S(V)$, and then we isochorically determine the difference in pressure between the isentrope and the Hugoniot using

$$P_H(V) = \frac{\left\{P_S(V) - \frac{\gamma}{V}(\Delta E_S + E_{\rm tr})\right\}}{\left\{1 - \left(\frac{\gamma}{2}\right)\left(\frac{V_{00}}{V} - 1\right)\right\}}, \tag{8}$$

where P_H, V_{00}, γ, and $E_{\rm tr}$ are the Hugoniot pressure, initial volume of the shocked material, the Grüneisen parameter, and the phase transition energy at ambient pressure. The volume dependence of the Grüneisen parameter is assumed to be given by

$$\gamma = \gamma_0(V/V_0)^q, \tag{9}$$

In our calculations, we have used $q = 1$ and γ_0 between 1 and 2. The energy change along the principal isentrope (ΔE_S) is evaluated by numerically integrating

$$\Delta E_S = -\int_{V_0}^{V} P_S dV. \tag{10}$$

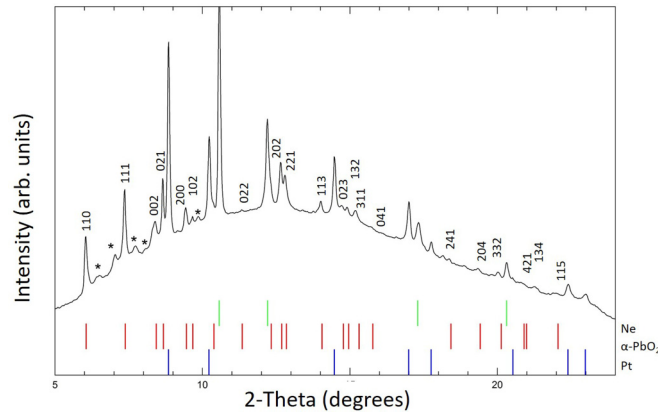

FIG. 1. X-ray-diffraction pattern at 51.0 GPa obtained upon quenching GeO_2 to room temperature after heating (~1700 K). Asterisks indicate peaks from the starting $P2_1/c$ phase. The ticks at the bottom represent the expected peak positions of platinum (blue), neon (green), and α-PbO_2-type GeO_2 (red). The Miller indices of α-PbO_2-type germania are indicated for the corresponding peaks.

The principal isentrope was assumed to have the form of the third-order Birch-Murnaghan equation of state.

K_S, the isentropic bulk modulus, and K'_S, its pressure derivative, are assumed to be related to the isothermal

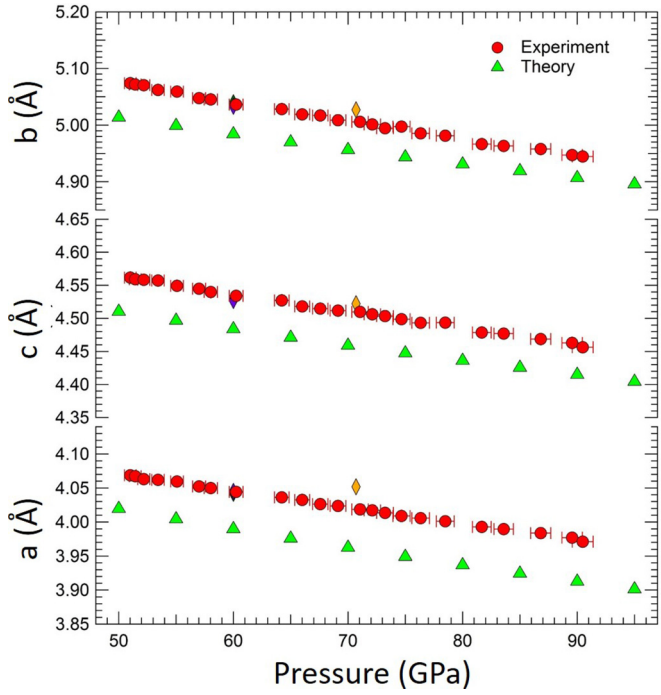

FIG. 2. Experimental (red circles) and calculated (green triangles) of α-PbO_2-type GeO_2 as a function of pressure at room temperature. Solid diamonds represent previous studies (yellow, Shiraki *et al.* [19]; purple, Prakapenka *et al.* [69]; green, Ono *et al.* [46]). The lattice parameters reported by Shiraki *et al.* [19] were obtained from experiments performed at high pressure and high temperature (70.7 GPa, 2110 K).

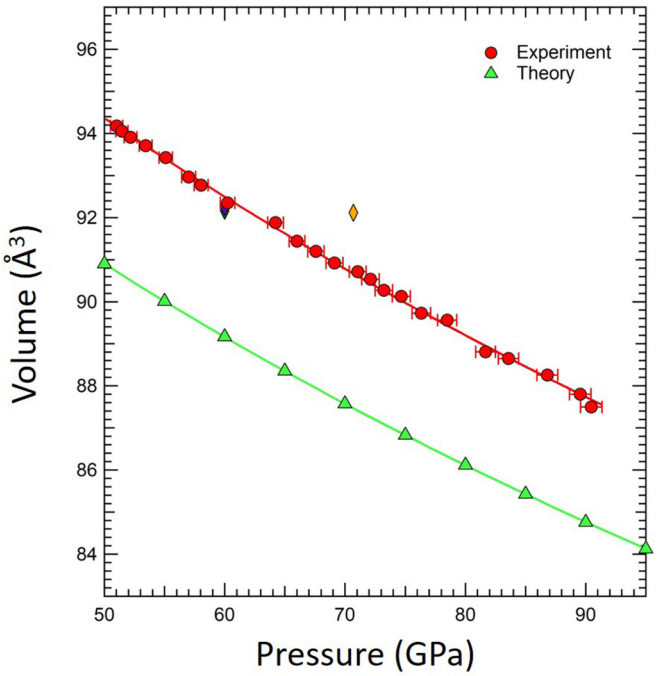

FIG. 3. Variation in unit cell volume of α-PbO_2-type GeO_2 with pressure (red circles: experiments; green triangles: theory). Solid lines are third-order Birch-Murnaghan fits to the data. Other symbols are defined in Fig. 2.

counterparts, K_T and K'_T, using

$$K_S = K_T(1 + \alpha\gamma T), \tag{11}$$

$$\left(\frac{\partial K_s}{\partial P}\right)_T \approx (1 + \alpha\gamma T)K'_T + \frac{\gamma T}{K_T}\left(\frac{\partial K_T}{\partial T}\right)_P, \tag{12}$$

$$K'_T = \left(\frac{\partial K_T}{\partial P}\right)_T, \tag{13}$$

$$K'_S = \left(\frac{\partial K_S}{\partial P}\right)_S = \left(\frac{\partial K_s}{\partial P}\right)_T + \left(\frac{\partial K_s}{\partial T}\right)_P \frac{\gamma T}{K_S}. \tag{14}$$

II. RESULTS

A. Equation of state

A GeO_2 sample was compressed at room temperature to 50.4 GPa. The 300-K diffraction pattern was consistent with a poorly crystalline monoclinic phase ($P2_1/c$) previously reported [18,22]. Upon heating to ~1700 K, new diffraction peaks appeared, and these peaks were retained upon quenching to room temperature after 30 min of heating time (*in situ* $P = 51.0$ GPa, Fig. 1). The measured d spacings could be fit to the α-PbO_2-type structure (see Supplemental Material [68], Table S1), which is the expected stable phase at these pressures [21]. The difference between our observed and calculated d spacings is less than <0.003 Å, indicating a good fit to the α-PbO_2-type structure. We then increased the pressure in 1–5-GPa steps with annealing at 1200 K (for ~5 min) at ~5-GPa intervals. Annealing was designed to reduce the differential stress. Figure 2 shows the lattice parameters obtained from both the experiments and theoretical calculations as a function of pressure up to 95 GPa. As expected, LDA underestimates the unit-cell dimensions with respect to experimentally obtained values. Our measured values are in good agreement with existing literature [46,69]. The experimental a, b, and c axial dimensions were found to decrease by 2.4, 2.6, and 2.3%, respectively, in the pressure range considered. The theoretically calculated parameters on the other hand decrease by 2.7, 2.1, and 2.1% between 50 and 90 GPa. However, the volume reductions obtained from the two methods are in good agreement (7.1 and 6.9% using experiments and theory, respectively).

Figure 3 shows the pressure-volume relation of α-PbO_2-type GeO_2. The EOS parameters are shown in Table I. Figure 4 (solid black lines) shows the covariance between K_{0T} and V_0 in the fitting results (1σ, 68.3% confidence). The negative slope of the confidence ellipse indicates the strong negative correlation between K_{0T} and V_0. The error bars indicate the estimated standard deviations of the two parameters.

We have examined the dependence of the fitting parameters on the choice of EOS of the platinum pressure standard. The EOS of Dewaele *et al.* [51] and Fei *et al.* [50] used as our primary pressure calibration is based on DAC data and cross-calibration of multiple standards up to 94 GPa. On the other hand, the pressure scale of Dorfman *et al.* [65] (data fit to BM-3) is calibrated over high pressures (to 250 GPa) using the MgO scale [70]. Using this EOS [65], we find that V_0 is 0.1% lower, while K_{0T} is 4.1% higher. Although not significantly different from our initial fitting parameters (Table I), it illustrates how modest differences in EOS

TABLE I. Equation of state parameters of the α-PbO_2- and $Pa\bar{3}$-type phases of GeO_2 and SiO_2.

		GeO_2 (This paper)			SiO_2		
Phase	Method	V_0(Å^3)	K_{0T} (GPa)	K'_{0T}	V_0(Å^3)	K_{0T} (GPa)	K'_{0T}
α-PbO_2	Experiment	53.8 (2)	293 (7)	4 (fixed)	45.8[a]	322 (2)[a]	4[a] (fixed)
	LDA	51.7	291	4.4	45.56[b]	324[b]	4.2[b]
		51.6	307	4 (fixed)			
$Pa\bar{3}$	Experiment	50.3 (3)	342 (12)	4 (fixed)	43.6 (2)[c]	348 (5)[c]	4[c] (fixed)
	LDA	48.8	313	4.4	43.5[b]	345[b]	4.3[b]
		48.3	351	4 (fixed)			

[a]Grocholski *et al.* [75].
[b]Oganov *et al.* [35].
[c]Kuwayama *et al.* [76].

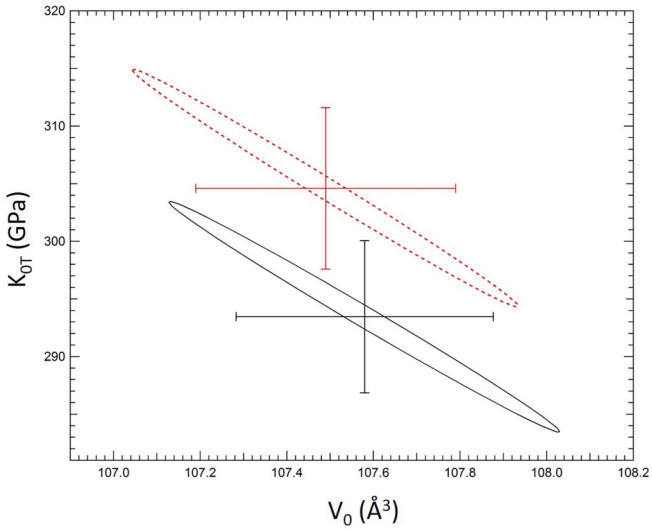

FIG. 4. Covariance (1σ) of the bulk modulus (K_{0T}) and the unit-cell volume (V_0) (experimental data) from equation of state fitting for the α-PbO_2-type phase. The two different covariance ellipses represent different Pt pressure scales (solid black, Dewaele *et al.* [51] and Fei *et al.* [50]; dashed red, Dorfman *et al.* [65]).

parameters for standards affect the final EOS of the material under study. The V_0 versus K_{0T} tradeoff curve for this case is also shown in Fig. 4 (red dashed lines).

An equation of state fit was also performed for the theoretical results both with and without fixing K'_{0T}. Table II lists the EOS parameters obtained from experiments and theory from this paper and previous studies on GeO_2 and SiO_2. Using $K'_{0T} = 4$ for both the experimental and theoretical data, LDA was found to underestimate V_0 by 4.0% and overestimate K_{0T} by 4.6%. Our estimated K_{0T} values (293 and 291 GPa using experiments and theory, respectively) are higher than reported by Prakapenka *et al.* [69], which was based on more limited pressure range (to 60 GPa) and lacked a pressure-transmitting medium.

A fresh sample was then prepared and compressed to 80.0 GPa at room temperature. Again, the ambient-temperature diffraction pattern could be assigned to the

TABLE II. Thermodynamic parameters of GeO_2 used for the calculation of the theoretical Hugoniot. The asterisk denotes an assumed value, HPP denotes the high-pressure phase observed on shock compression of rutile-type GeO_2 (Ref. [1]), γ_0 denotes the Grüneisen parameter, α denotes the thermal expansion coefficient, and E_{TR} denotes phase transition energy. The subscript 0 indicates zero-pressure conditions.

Phase	γ_0	q	α (10^{-5} K^{-1})	E_{tr} (kJ/g)
Rutile	1.16[a]	1*	2.03[b]	–
$CaCl_2$	1, 2*	1*	2.05*	0
α-PbO_2	1, 2*	1*	2.05*	+0.07
$Pa\bar{3}$	1, 2*	1*	2.05*	+0.21
HPP[c]	1.24[c]	0[c]		+0.1[c]

[a]Wang and Simmons [81].
[b]Hazen and Finger [82].
[c]Jackson and Ahrens [1].

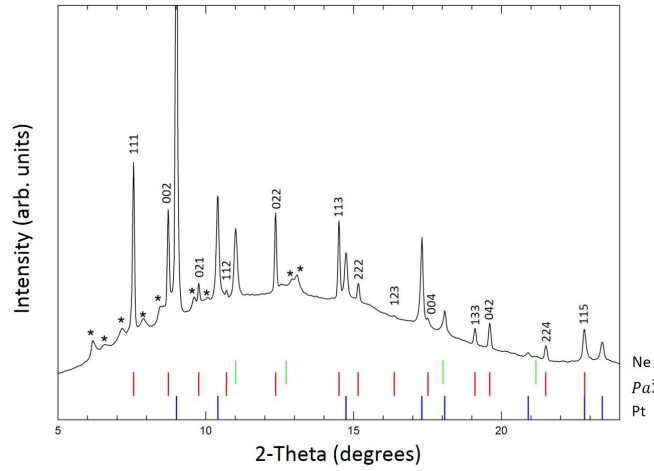

FIG. 5. X-ray-diffraction pattern at 82.8 GPa obtained upon quenching GeO_2 to ambient temperature after heating (~1690 K). Ticks at the bottom indicate the simulated peak positions of platinum (blue), neon (green), and $Pa\bar{3}$-type GeO_2 (red). Miller indices of $Pa\bar{3}$-type germania are shown next to the corresponding diffraction peaks. Asterisks indicate peaks from the $P2_1/c$ phase.

$P2_1/c$ monoclinic phase. On heating at ~1690 K, new x-ray-diffraction peaks were observed. The temperature-quenched diffraction pattern after 20-min heating could be indexed using the $Pa\bar{3}$-type structure (see Supplemental Material [68], Table S2). Figure 5 shows the diffraction pattern obtained on quenching from the peak temperature (*in situ* $P = 82.8$ GPa). The sample was then further compressed to 119.5 GPa resulting in a 1.7% decrease in unit-cell parameter over this

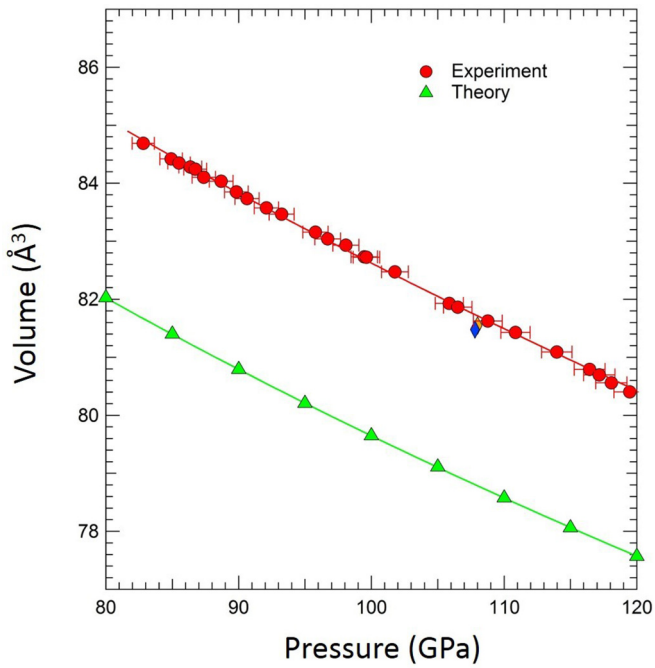

FIG. 6. Change in the unit-cell volume of $Pa\bar{3}$-type GeO_2 as a function of pressure. Solid lines are third-order Birch-Murnaghan fits to the data (red, experiments; green, theory). Literature data (yellow, Shiraki *et al.* [19]; blue, Ono *et al.* [46]) are represented by the solid diamonds.

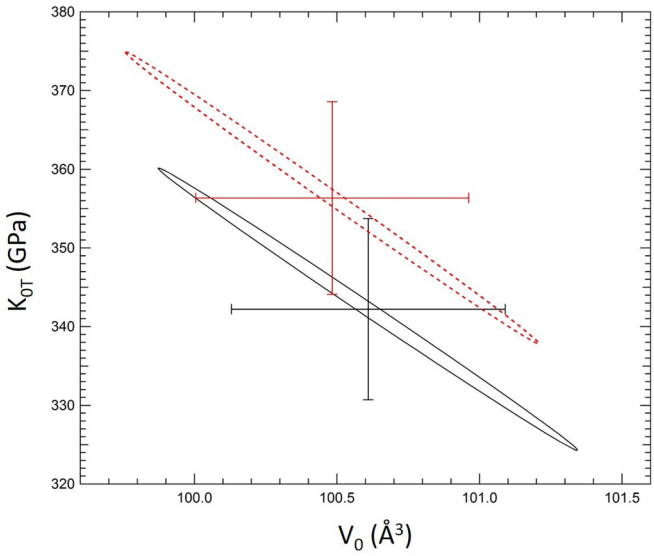

FIG. 7. Covariance (1σ) of the bulk modulus (K_{0T}) and the unit-cell volume (V_0) from equation of state fitting for the $Pa\bar{3}$-type phase (experimental data). Red and black ellipses have the same meaning as in Fig. 4.

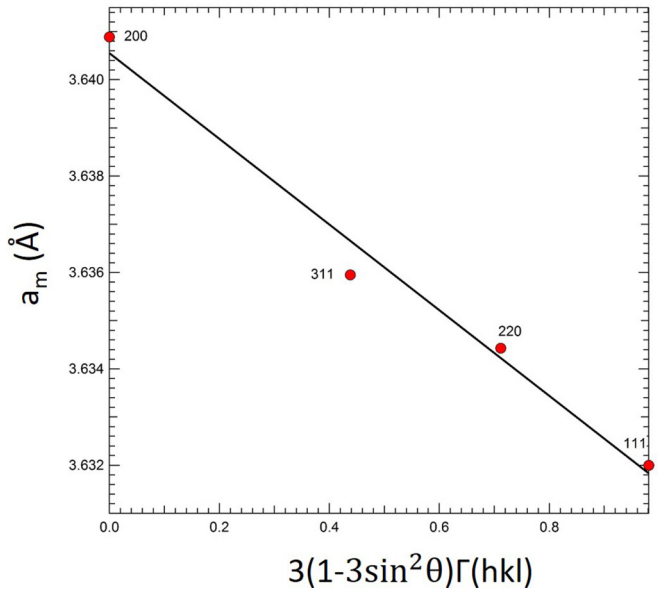

FIG. 8. Lattice parameter variation of platinum determined from individual (*hkl*) values at 113.9 GPa.

range. The LDA calculations systematically underestimate the lattice parameter as also observed for the α-PbO_2-type phase. However, theory and experiment show a similar pressure dependence as the theoretically calculated lattice parameter decreases by 1.8% between 80 and 120 GPa. Figure 6 shows the pressure-volume relation obtained from this paper as well as limited data available from previous experimental studies [19,46]. Using a third-order Birch-Murnaghan fit to our experimental data, the EOS parameters are $V_0 = 100.6\,(5)$ Å^3, $K_{0T} = 342\,(12)$ GPa, and $K'_{0T} = 4$ (fixed). At 108 GPa, our cell volume (81.68 Å^3) is in good agreement with Shiraki *et al.* [19] (81.54 Å^3) and Ono *et al.* [46] (81.48 Å^3). Figure 8 shows the covariance (1σ) of K_{0T} and V_0 for the experimental data. In case of the theoretical data, V_0 and K_{0T} are underestimated and overestimated by 3.9 and 2.7%, respectively. Table I summarizes the EOS parameters obtained from both experiments and theory and compares it to available experimental and theoretical data. Figure 7 shows the correlation ellipses for V_0 and K_{0T} using the platinum EOS parameters of Dewaele *et al.* [51] and Fei *et al.* [50] (solid black) and Dorfman *et al.* [65] (red dashed). In the latter case, the fitting parameters V_0 and K_{0T} are 0.1 and 4.1% higher and lower, respectively.

B. Differential stress

Figure 8 shows an example of variation of the measured lattice parameter (a_m) with $3(1-3\sin^2\theta)\Gamma(hkl)$ for Pt at 113.8 GPa. The data points can be fit well using a straight line. The negative slope of the line is consistent with the orientation of anisotropy in Pt [66], and thus the variations in lattice parameter are consistent with effects of differential stress. Using the slope and intercept of the Γ plots, we calculated the differential stress as a function of pressure and compared it with previous experiments on Pt in a Ne medium [65] and without any medium [71] (Fig. 9). The differential stress increases with pressure from ~0.7 GPa at 52 GPa to ~2.6 GPa at the peak pressure (119.5 GPa).

Our results are consistent with previous work on Pt using a Ne medium [65] and lie below reported values of t when

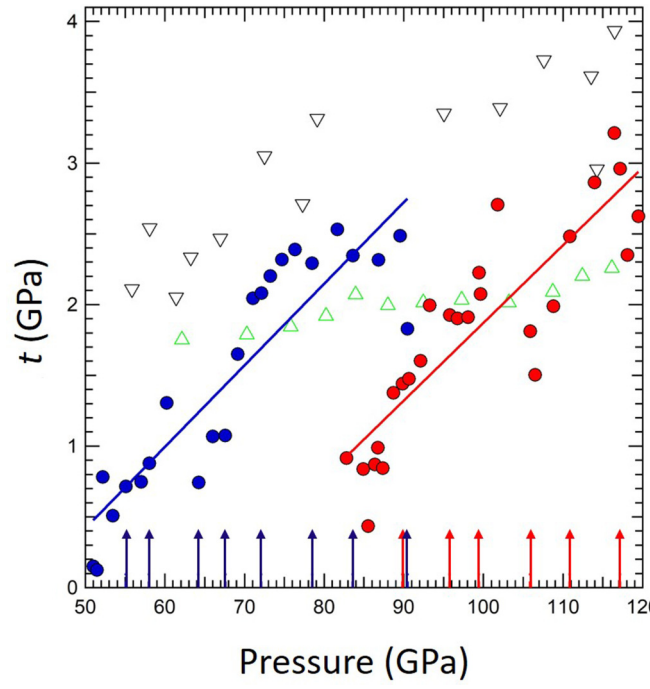

FIG. 9. Differential stress t in platinum as a function of pressure (solid blue, α-PbO_2 cell; solid red, $Pa\bar{3}$-type cell). The green open triangles show Pt in a neon pressure medium [65] and the black inverted triangles are for platinum in the absence of a pressure medium [71]. The solid red and blue lines are linear fits to our data for the respective phases. The blue and red arrows show laser annealing for the respective phase.

no medium is used [71]. This indicates that Pt has not yet reached its yield point, so our values provide a reasonable estimate of the differential stress in the sample. In general agreement with previous observations [65] t is ~2% of the total pressure at megabar conditions. The low differential stress in platinum indicates that quasihydrostatic conditions were maintained in the DAC up to the peak pressure. The effects of laser annealing can also be observed in this data as differential stress tends to drop immediately after laser heating (Fig. 9). Differential stresses could not be directly evaluated in the cubic phase of GeO_2 due to lack of reported single-crystal elasticity data.

C. Comparison with shock compression data

The behavior of GeO_2 under dynamic compression has also attracted interest [1,2,24,25,72]. Gas gun shock-wave experiments [1] on rutile-type and amorphous GeO_2 have been interpreted to indicate a phase transition to a high-pressure phase at $P > 70$ and >35 GPa, respectively. However, the structure of the HPP could not be directly determined in these experiments.

Figure 10 shows the theoretical Hugoniots assuming the rutile phase as an initial state and transforming to the different possible high-pressure phases of GeO_2. The Hugoniot of SiO_2 stishovite [73] is shown for comparison. The parameters used for the calculations are summarized in Table II. In agreement with Jackson and Ahrens [1], the low-pressure region (up to ~50 GPa) can be well described with the rutile-type phase and thus there is no evidence of a phase transition up to this pressure. The data at 70–90 GPa are generally consistent with a theoretical Hugoniot calculated assuming either the $CaCl_2$- or the α-PbO_2-type phase as the HPP. The highest-pressure datum (165.5 GPa) is not consistent with the predicted Hugoniots of any of the high-pressure phases of GeO_2 and may represent melt. The $Pa\bar{3}$-type phase can be ruled out as a candidate HPP as it is predicted to be much denser along the Hugoniot than the experimental data.

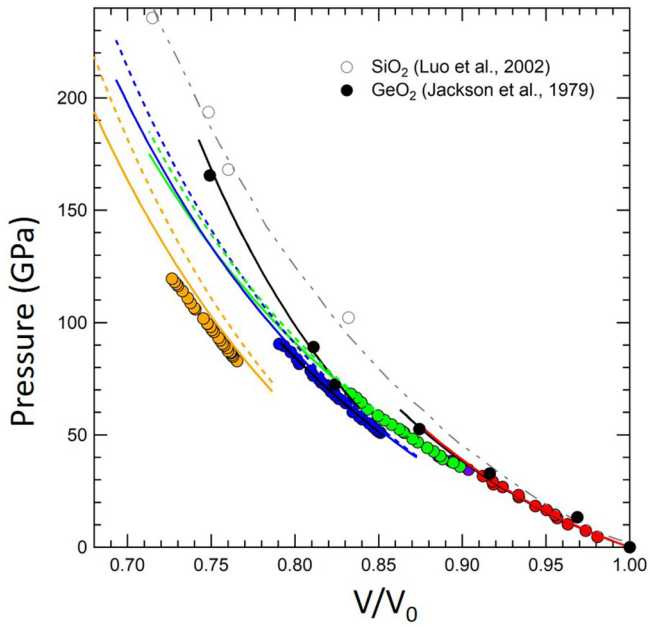

FIG. 10. Theoretical Hugoniot for the rutile- (red), $CaCl_2$- (green), α-PbO_2- (blue), and $Pa\bar{3}$-type (yellow) GeO_2. Solid and dashed colored lines are for cases where $\gamma = 1$ and 2, respectively. Black circles and lines are the shock data and the fit of Jackson and Ahrens [1] for GeO_2 starting from the rutile structure. V_0 refers to the ambient-pressure volume of the rutile-type phase (55.33 $Å^3$). Open gray symbols are shock data for stishovite (rutile-type SiO_2), from Luo *et al.* [73].

III. DISCUSSION

The data reported here provide detailed 300-K equations of state for the high-pressure α-PbO_2- and $Pa\bar{3}$-type phases of GeO_2. Our results are consistent with limited previous data and enable us to constrain EOS parameters for these materials. The equations of state of GeO_2 phases provide a benchmark for theoretical calculations and are of interest for comparison with the behavior of SiO_2 (see below). Crystalline GeO_2 equation of state data also have applications in interpretation of experimental studies of GeO_2 glass by x-ray-absorption spectroscopy [4,7] and x-ray diffraction [13] as well as by theoretical molecular dynamics simulations [48].

Figure 11 compares the measured 300-K pressure-volume relationships across four phases of GeO_2 and SiO_2 [74–76]. Because of the larger size of the Ge^{4+} cation in comparison to Si^{4+}, GeO_2 has a larger unit-cell volume but SiO_2 and GeO_2 follow the same phase transition sequence. The rutile (stishovite) to $CaCl_2$-type phase transition is second order [74,77] with almost no volume change. A detailed study of the equation of state of the rutile and $CaCl_2$-type phases of GeO_2 will be published separately [78]. In the case of SiO_2, the $CaCl_2$ to α-PbO_2-type phase transition leads to a 0.6% reduction in molar volume [32], while the α-PbO_2-type to $Pa\bar{3}$-type phase transition involves a 5% volume change

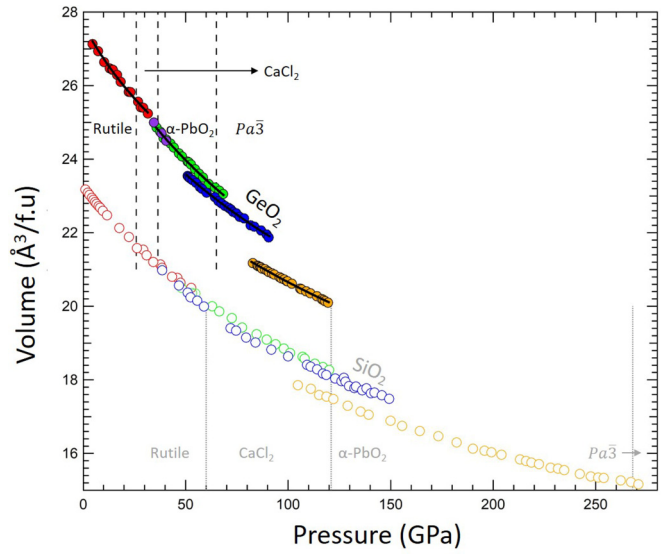

FIG. 11. Unit-cell volume of the rutile- (red), $CaCl_2$- (green), α-PbO_2- (blue), and $Pa\bar{3}$-type (yellow) phases of GeO_2 (solid) and SiO_2 (unfilled) [74–76]. Purple data points indicate rutile-type phase data that were not used for the EOS fit. The black and gray dashed lines indicate the phase boundaries in GeO_2 and SiO_2, respectively. The solid black lines are third-order Birch-Murnaghan fits to the data.

[33]. Using our equation of state parameters, we determine the volume change to be 1.9 and 1.3% for the $CaCl_2$-type to α-PbO_2-type transition from experiments and theory, respectively (assuming transition pressure = 36 GPa). In case of the α-PbO_2-type to $Pa\bar{3}$-type transition, the volume reduction is 4.8 and 4.9% for experiments and theory, respectively (assuming transition pressure = 65 GPa), which is similar to the volume change in SiO_2.

Table I lists the EOS parameters for the α-PbO_2- and $Pa\bar{3}$-type phases of both SiO_2 and GeO_2 from both experiments and theoretical calculations. For the α-PbO_2-type phase, the zero-pressure bulk modulus of GeO_2 is ~9% lower than that of the SiO_2 phase. However, the experimental data suggest that the bulk moduli of GeO_2 and SiO_2 in the $Pa\bar{3}$-type phase may be more similar. Based on our experimental equation of state date, the zero-pressure bulk modulus of the $Pa\bar{3}$-type phase is about 16% larger than that of the α-PbO_2-type phase.

Shock compression experiments on fused silica and α-quartz indicate transitions to stishovite and/or stishovite-like phase(s) at ~35 GPa [41,79] with melting occurring above ~70 and ~110 GPa, respectively [80]. Direct shock compression experiments [73] on stishovite starting material do not show any evidence for phase transitions up to ~235 GPa. We calculated the theoretical Hugoniot of the different phases of GeO_2 based on rutile-type starting material. Our calculations suggest that the high-pressure phase observed on shock compression of vitreous and rutile-type germania can be interpreted as either the $CaCl_2$- or α-PbO_2-type phase.

IV. CONCLUSIONS

Using laser-heated diamond anvil cell experiments and theoretical calculations based on density functional theory, we have determined the lattice parameter(s) of α-PbO_2- and $Pa\bar{3}$-type GeO_2 up to 1.2 Mbars. The pressure-volume data were fit to the third-order Birch-Murnaghan equation of state. Our experimental and theoretical data are in good agreement. The experimental and theoretical data for the α-PbO_2-type phase can be fit using $V_0 = 53.8\,(2)$ Å^3, $K_{0T} = 293\,(7)$ GPa; $V_0 = 51.6$ Å^3, $K_{0T} = 307$ GPa; and $K'_{0T} = 4$ (fixed), respectively. In case of the $Pa\bar{3}$-type phase, the EOS parameters obtained from fitting the experimental and theoretical data are $V_0 = 50.3\,(3)$ Å^3, $K_{0T} = 342\,(12)$ GPa; $V_0 = 48.3$ Å^3, $K_{0T} = 351$ GPa; and $K'_{0T} = 4$ (fixed), respectively. Nonhydrostatic stress analysis of Pt shows that the differential stress in the cells was low (~2% at the peak pressure) and quasihydrostatic conditions were maintained. The effect of choosing different Pt pressure standards on the equation of state of GeO_2 has also been evaluated.

ACKNOWLEDGMENTS

The authors are grateful to S. J. Tracy, C. V. Stan, J. K. Wicks, and S. Tkachev for helpful comments on the paper and/or experimental assistance. The work was funded by the NSF (Grant No. EAR-1415321). Use of the Advanced Photon Source, an Office of Science User Facility, US Department of Energy (DOE) is acknowledged. GeoSoilEnviroCARS (GSECARS, Sector 13), is supported by the NSF Earth Sciences (Grant No. EAR-1634415) and the DOE, Geosciences (Grant No. DE-FG02-94ER14466). The gas-loading facility at GSECARS is partially supported by the Consortium for Materials Properties Research in Earth Sciences under NSF Cooperative Agreement EAR Grant No. 1606856. This research used resources of the Advanced Photon Source, operated for the DOE Office of Science by Argonne National Laboratory under Contract No. DE-AC02-06CH11357.

[1] I. Jackson and T. J. Ahrens, Phys. Earth Planet. Inter. **20**, 60 (1979).
[2] C. Liu, T. J. Ahrens, and N. S. Brar, J. Appl. Phys. **91**, 9136 (2002).
[3] M. Micoulaut, L. Cormier, and G. S. Henderson, J. Phys.: Condens. Matter **18**, R753 (2006).
[4] X. Hong, G. Shen, V. B. Prakapenka, M. Newville, M. L. Rivers, and S. R. Sutton, Phys. Rev. B **75**, 104201 (2007).
[5] M. Vaccari, G. Aquilanti, S. Pascarelli, and O. Mathon, J. Phys.: Condens. Matter **21**, 145403 (2009).
[6] M. Baldini, G. Aquilanti, H.-k. Mao, W. Yang, G. Shen, S. Pascarelli, and W. L. Mao, Phys. Rev. B **81**, 024201 (2010).
[7] X. Hong, M. Newville, T. S. Duffy, S. R. Sutton, and M. L. Rivers, J. Phys.: Condens. Matter **26**, 035104 (2014).
[8] D. J. Durben and G. H. Wolf, Phys. Rev. B **43**, 2355 (1991).
[9] P. V. Teredesai, D. T. Anderson, N. Hauser, K. Lantzky, and J. L. Yarger, Phys. Chem. Glasses **46**, 345 (2005).
[10] M. Guthrie, C. A. Tulk, C. J. Benmore, J. Xu, J. L. Yarger, D. D. Klug, J. S. Tse, H.-k. Mao, and R. J. Hemley, Phys. Rev. Lett. **93**, 115502 (2004).
[11] Q. Mei, S. Sinogeikin, G. Shen, S. Amin, C. J. Benmore, and K. Ding, Phys. Rev. B **81**, 174113 (2010).
[12] G. Lelong, L. Cormier, G. Ferlat, V. Giordano, G. S. Henderson, A. Shukla, and G. Calas, Phys. Rev. B **85**, 134202 (2012).
[13] Y. Kono, C. Kenney-Benson, D. Ikuta, Y. Shibazaki, Y. Wang, and G. Shen, Proc. Natl. Acad. Sci. USA **113**, 3436 (2016).
[14] J. A. Erwin Desa, A. C. Wright, and R. N. Sinclair, J. Non-Cryst. Solids **99**, 276 (1988).
[15] J. W. E. Drewitt, P. S. Salmon, A. C. Barnes, S. Klotz, H. E. Fischer, and W. A. Crichton, Phys. Rev. B **81**, 014202 (2010).
[16] P. S. Salmon, J. W. E. Drewitt, D. A. J. Whittaker, A. Zeidler, K. Wezka, C. L. Bull, M. G. Tucker, M. C. Wilding, M. Guthrie, and D. Marrocchelli, J. Phys.: Condens. Matter **24**, 415102 (2012).
[17] J. Haines, J. M. Léger, C. Chateau, and A. S. Pereira, Phys. Chem. Min **27**, 575 (2000).
[18] J. Haines, J. M. Léger, and C. Chateau, Phys. Rev. B **61**, 8701 (2000).
[19] K. Shiraki, T. Tsuchiya, and S. Ono, Acta Crystallogr. Sect. B **59**, 701 (2003).
[20] S. Ono, K. Hirose, N. Nishiyama, and M. Isshiki, Am. Miner **87**, 99 (2002).
[21] S. Ono, T. Tsuchiya, K. Hirose, and Y. Ohishi, Phys. Rev. B **68**, 134108 (2003).

[22] V. B. Prakapenka, G. Shen, L. S. Dubrovinsky, M. L. Rivers, and S. R. Sutton, J. Phys. Chem. Solids **65**, 1537 (2004).

[23] N. Suresh, G. Jyoti, S. C. Gupta, S. K. S. Sangeeta, and S. C. Sabharwal, J. Appl. Phys. **76**, 1530 (1994).

[24] S. S. Batsanov, E. V. Lazareva, and L. I. Kopaneva, Zh. Neorg. Khim **23**, 1754 (1978).

[25] I. Rosales, C. Thions-Renero, E. Martinez, L. Bucio, and E. Orozco, High Press. Res. **31**, 428 (2011).

[26] Z. Łodziana, K. Parlinski, and J. Hafner, Phys. Rev. B **63**, 134106 (2001).

[27] K. V. Shanavas, N. Garg, and S. M. Sharma, Phys. Rev. B **73**, 094120 (2006).

[28] D. Marrocchelli, M. Salanne, and P. A. Madden, J. Phys.: Condens. Matter **22**, 152102 (2010).

[29] H. Dekura, T. Tsuchiya, and J. Tsuchiya, Phys. Rev. B **83**, 134114 (2011).

[30] Y. Tsuchida and T. Yagi, Nature (London) **340**, 217 (1989).

[31] D. Andrault, G. Fiquet, F. Guyot, and M. Hanfland, Science **282**, 720 (1998).

[32] M. Murakami, K. Hirose, S. Ono, and Y. Ohishi, Geophys. Res. Lett. **30**, 1207 (2003).

[33] Y. Kuwayama, K. Hirose, N. Sata, and Y. Ohishi, Science **309**, 923 (2005).

[34] T. Tsuchiya and J. Tsuchiya, Proc. Natl. Acad. Sci. USA **108**, 1252 (2011).

[35] A. R. Oganov, M. J. Gillan, and G. D. Price, Phys. Rev. B **71**, 064104 (2005).

[36] T. Duffy, N. Madhusudhan, and K. K. M. Lee, in *Treatise on Geophysics*, 2nd ed., edited by G. Schubert (Elsevier, Oxford, 2015), pp. 149–178.

[37] C. Prescher, V. B. Prakapenka, J. Stefanski, S. Jahn, L. B. Skinner, and Y. Wang, Proc. Natl. Acad. Sci. USA **114**, 10041 (2017).

[38] S. Petitgirard, High Press. Res. **37**, 200 (2017).

[39] C. Meade and R. Jeanloz, Science **241**, 1072 (1988).

[40] T. Sato and N. Funamori, Phys. Rev. Lett. **101**, 255502 (2008).

[41] S. J. Tracy, S. J. Turneaure, and T. S. Duffy, Phys. Rev. Lett. **120**, 135702 (2018).

[42] S. Ono, K. Funakoshi, A. Nozawa, and T. Kikegawa, J. Appl. Phys. **97**, 073523 (2005).

[43] B. Zhu, C.-M. Liu, M.-B. Lv, X.-R. Chen, J. Zhu, and G.-F. Ji, Physica B **406**, 3508 (2011).

[44] B. Grocholski, S.-H. Shim, E. Cottrell, and V. B. Prakapenka, Am. Miner **99**, 170 (2014).

[45] M. Madon, P. Gillet, C. Julien, and G. D. Price, Phys. Chem. Minerals **18**, 7 (1991).

[46] S. Ono, T. Tsuchiya, K. Hirose, and Y. Ohishi, Phys. Rev. B **68**, 014103 (2003).

[47] J. P. Itie, A. Polian, G. Calas, J. Petiau, A. Fontaine, and H. Tolentino, Phys. Rev. Lett. **63**, 398 (1989).

[48] V. V. Brazhkin, A. G. Lyapin, and K. Trachenko, Phys. Rev. B **83**, 132103 (2011).

[49] J. D. Jorgensen, J. Appl. Phys. **49**, 5473 (1978).

[50] Y. Fei, A. Ricolleau, M. Frank, K. Mibe, G. Shen, and V. Prakapenka, Proc. Natl. Acad. Sci. USA **104**, 9182 (2007).

[51] A. Dewaele, P. Loubeyre, and M. Mezouar, Phys. Rev. B **70**, 094112 (2004).

[52] V. B. Prakapenka, A. Kubo, A. Kuznetsov, A. Laskin, O. Shkurikhin, P. Dera, M. L. Rivers, and S. R. Sutton, High Press. Res. **28**, 225 (2008).

[53] A. P. Jephcoat and S. P. Besedin, Phil. Trans. R. Soc. A **354**, 1333 (1996).

[54] C. Prescher and V. B. Prakapenka, High Press. Res. **35**, 223 (2015).

[55] T. J. B. Holland and S. A. T. Redfern, Mineral. Mag. **61**, 65 (1997).

[56] P. Hohenberg and W. Kohn, Phys. Rev. **136**, B864 (1964).

[57] W. Kohn and L. J. Sham, Phys. Rev. **140**, A1133 (1965).

[58] S. J. Clark, M. D. Segall, C. J. Pickard, P. J. Hasnip, M. I. J. Probert, K. Refson, and M. C. Payne, Z. Kristallogr. **220**, 567 (2009).

[59] H. J. Monkhorst and J. D. Pack, Phys. Rev. B **13**, 5188 (1976).

[60] D. Vanderbilt, Phys. Rev. B **41**, 7892 (1990).

[61] C. G. Broyden, IMA J. Appl. Math. **6**, 222 (1970).

[62] A. K. Singh, J. Appl. Phys. **73**, 4278 (1993).

[63] A. K. Singh and T. Kenichi, J. Appl. Phys. **90**, 3269 (2001).

[64] A. K. Singh, J. Appl. Phys. **106**, 043514 (2009).

[65] S. M. Dorfman, V. B. Prakapenka, Y. Meng, and T. S. Duffy, J. Geophys. Res. **117**, B08210 (2012).

[66] E. Menéndez-Proupin and A. K. Singh, Phys. Rev. B **76**, 054117 (2007).

[67] P. D. Asimow, in *Treatise on Geophysics*, 2nd ed., edited by G. Schubert (Elsevier, Oxford, 2015), pp. 393–416.

[68] See Supplemental Material at http://link.aps.org/supplemental/10.1103/PhysRevB.98.144106 for data used in performing the EOS fittings.

[69] V. B. Prakapenka, L. S. Dubrovinsky, G. Shen, M. L. Rivers, S. R. Sutton, V. Dmitriev, H.-P. Weber, and T. L. Bihan, Phys. Rev. B **67**, 132101 (2003).

[70] T. Yoshinori, N. Yu, and T. Taku, J. Geophys. Res. **114**, B03208 (2009).

[71] A. K. Singh, H.-P. Liermann, Y. Akahama, S. K. Saxena, and E. Menéndez-Proupin, J. Appl. Phys. **103**, 063524 (2008).

[72] G. Q. Chen, T. J. Ahrens, W. Yang, and J. K. Knowles, J. Mech. Phys. Solids **47**, 763 (1999).

[73] S. N. Luo, J. L. Mosenfelder, P. D. Asimow, and T. J. Ahrens, Geophys. Res. Lett. **29**, 36 (2002).

[74] D. Andrault, R. J. Angel, J. L. Mosenfelder, and T. L. Bihan, Am. Miner **88**, 301 (2003).

[75] B. Grocholski, S.-H. Shim, and V. B. Prakapenka, J. Geophys. Res. B **118**, 4745 (2013).

[76] Y. Kuwayama, K. Hirose, N. Sata, and Y. Ohishi, Phys. Chem. Miner. **38**, 591 (2011).

[77] C. Lee and X. Gonze, J. Phys.: Condens. Matter **7**, 3693 (1995).

[78] R. Dutta, V. B. Prakapenka, and T. S. Duffy (unpublished).

[79] S. P. Marsh, *LASL Shock Hugoniot Data* (University of California, Berkeley, 1980).

[80] G. A. Lyzenga, T. J. Ahrens, and A. C. Mitchell, J. Geophys. Res. **88**, 2431 (1983).

[81] H. Wang and G. Simmons, J. Geophys. Res. **78**, 1262 (1973).

[82] R. M. Hazen and L. W. Finger, J. Phys. Chem. Solids **42**, 143 (1981).